X-524-72-412
PREPRINT

PHOTODIODES FOR TEN MICROMETER LASER COMMUNICATION SYSTEMS

STEVEN C. COHEN

OCTOBER 1972

GSFC
GODDARD SPACE FLIGHT CENTER
GREENBELT, MARYLAND

X-524-72-412
Preprint

PHOTODIODES FOR TEN MICROMETER LASER COMMUNICATION SYSTEMS

Steven C. Cohen

October 1972

Goddard Space Flight Center
Greenbelt, Maryland

PHOTODIODES FOR TEN MICROMETER
LASER COMMUNICATION SYSTEMS

ABSTRACT

This document discusses the performance of 10 μm mercury-cadmium-telluride and lead-lin-telluride photodiodes in laser heterodyne communication systems. We examine the dependence of detector quantum efficiency, resistance, frequency response, and signal-to-noise ratio on temperature, bias, and local oscillator power. Included in the discussion is an analysis of the feasibility of high temperature operation (> 150°k), and ability of the detector to dissipate power to a heat sink is explored. Some aspects of direct detection response are considered and figures showing flux levels from a blackbody presented.

CONTENTS

ILLUSTRATIONS

CONTENTS

ILLUSTRATIONS–(continued)

TABLES

PHOTODIODES FOR TEN MICROMETER LASER COMMUNICATION SYSTEMS

I. INTRODUCTION

This document presents results of computer-aided calculations of the performance of 10 μm photodiodes for satellite-borne laser communication systems. The two candidate detector materials are mercury-cadium-telluride and lead-tin-telluride. Both are compound semiconductors with energy gaps which vary with temperature and mole fraction of constituent molecules. They have potential for gigahertz bandwidths and in heterodyne detection systems have quantum noise limited operation with 5 milliwatts or less of local oscillator power. In this presentation, we examine the dependence of detector quantum efficiency, resistance, frequency response, and signal-to-noise ratio on temperature, bias, and local oscillator power. The effect of various doping concentrations and detector size is examined. We also show the dependence of detectivity and related direct detection characteristics on temperature. Included in the discussion is an analysis of the feasibility of high temperature (> 150°K) detectors, and figures of background flux levels due to a blackbody. The ability of the detector to dissipate power to a heat sink is examined. The analysis is based on the classical model of a p-n homojunction. Accordingly, comments on performance of heterojunctions and diodes using the Burstein-Moss effect are not included here although many of our remarks are equally applicable to the more novel diodes.

II. SIGNAL-TO-NOISE RATIO, DERIVATION

The suitability of a detector for use in a laser communication system can be analyzed by way of the signal-to-noise ratio expected at the device output. This requires knowledge of device equivalent circuit, detection technique (e.g. direct, heterodyne), material parameters such as energy gap and dielectric constant, and external parameters such as temperature and bias.

The equivalent circuit for a photodiode is shown in Fig. 1. The junction conductance is G_D, its resistance is R_D, and its capacitance, C. The parasite series resistance (plus the load resistance across the output) is R_s, and ω is the angular frequency of the signal. From Fig. 1, it follows that the real part of the diode output admittance, G, is[1]

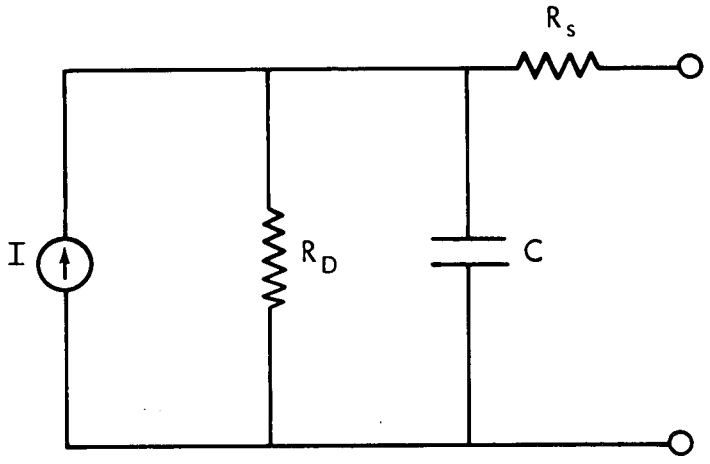

Figure 1. Equivalent Circuit of Photodiode

$$G = \frac{G_D + R_S (G_D^2 + \omega^2 C^2)}{(1 + G_D R_S)^2 + (\omega C R_S)^2} ; \tag{1}$$

hence the output impedance, R is

$$R = \frac{(1 + G_D R_S)^2 + (\omega C R_S)^2}{G_D + R_S (G_D^2 + \omega^2 C^2)} . \tag{2}$$

We will use Eq. (2) at several points in our analysis.

In analyzing the signal-to-noise ratio there are four important noise mechanisms which must be considered. The first of these, thermal noise, arises from thermally-induced fluctuations in charge carrier kinetic energy. The mean squared thermal noise current, i_{th}^2 , is

$$i_{th}^2 = \frac{4 k T B}{R} \tag{3}$$

where k is Boltzman's constant, T is the temperature, and B is the noise bandwidth. To this, we add the statistically independent amplifier noise

$$i_A^2 = \frac{4 k T' B}{R} \tag{4}$$

where T' is the temperature of amplifier at the detector output. A third source of noise is the granularity of the d.c. current, $I_{d.c.}$. The associated shot noise is

$$i_{sh}^2 = \frac{2 e I_{d.c.} B}{(1 + G_D R_S)^2 + (\omega C R_S)^2} \tag{5}$$

where e is the magnitude of the electronic charge and $I_{d.c.}$ is the total d.c. current including dark and photo components:

$$I_{d.c.} = I_D + I_B + I_S + I_{LO} \tag{6}$$

where I_D, I_B, I_S, I_{LO} are the d.c. currents in the dark and due to background radiation, signal radiation, and local oscillator radiation respectively. At low frequencies, a fourth noise, known as 1/f or flicker noise must be considered. It takes the functional form

$$i_{1/f}^2 = \frac{A I_{d.c.}^2}{f^n} B \tag{7}$$

with A and n constants ($n \approx 1$). In general, 1/f noise is negligible at frequencies used in communication. It will not be considered further in this paper.

The mean squared signal current, i_s^2, in the diode depends on the mode of detection. In direct detection

$$i_s^2 = \frac{\left(\frac{e \eta P_S}{h \nu}\right)^2}{(1 + G_D R_S)^2 + (\omega C R_S)^2} \tag{8}$$

where η is the detector quantum efficiency, P_s is the received signal power, h is Planck's constant, and ν is the light frequency. The signal-to-noise ratio for direct detection is

$$\left(\frac{S}{N}\right)_D = \frac{\left(\frac{e\,\eta\,P_S}{h\nu}\right)^2}{2e\,I_{d.c.}\,B + 4K(T+T')\,(G_D + R_S(G_D^2 + \omega^2 C^2))\,B} \tag{9}$$

In heterodyne detection, the signal at the intermediate frequency is

$$i_S^2 = \frac{2\left(\frac{e\,\eta}{h\nu}\right)^2 P_S\,P_{L.O.}}{(1 + G_D\,R_S)^2 + (\omega\,C\,R_S)^2} \tag{10}$$

where $P_{L.O.}$ is the local oscillator power. The signal-to-noise ratio at the i.f. frequency is

$$\left(\frac{S}{N}\right)_H = \frac{2\left(\frac{e\,\eta}{h\nu}\right)^2 P_S\,P_{L.O.}}{2e\,I_{d.c.}\,B + 4K(T+T')\,(G_D + R_S(G_D^2 + \omega^2 C^2))\,B}\,. \tag{11}$$

The material parameters of the photosensing substance determine η, $I_{d.c.}$, G_D, C and detector frequency response. These parameters are functions of the temperature, bias, and radiation intensity. Before examining their detailed behavior we wish to write down a few limiting forms of Eqs. 9 and 11. Using $I_S = e\eta P_S/h\nu$, we find for direct detection

$$\left(\frac{S}{N}\right)_D = \frac{\eta P_S}{2h\nu B}\left\{\frac{I_{d.c.}}{I_S} + \frac{2K(T+T')}{I_S\,R_D}\,(1 + R_S(G_D + \omega^2 C^2\,R_S))\right\}^{-1}. \tag{12}$$

If the two major contributors to the d.c. current are dark current and photocurrent due to ϕ background photons/area/second arriving at the detector then $I_{d.c.} = J_D\,A + e\eta\phi A$ where J_D is the dark current density and A is the detector surface area. The important figure of merit, the detectivity, D*, is the reciprocal of the noise equivalent power normalized to unit area and unit band. Therefore, setting $(S/N)_D$, A, and B equal to unity (and assuming $(\omega c)^2 < 1/R_D R_S$

$$D^* = \frac{1}{h\nu}\left\{\frac{\eta^2 e^2}{2\ e J_D + \eta e^2 \phi + \frac{4K(T+T')}{R_D}\ (1 + G_D R_S)}\right\}^{1/2} \tag{13}$$

When background generated shot noise dominates all other noise terms, we get the background limited detectivity

$$D^*_{B11p} = \frac{1}{h\nu}\sqrt{\frac{\eta}{2\phi}}\,. \tag{14}$$

The background limited detectivity is plotted in Fig. 2 as a function of blackbody temperature for several quantum efficiencies.

In the case of heterodyne detection, we assume that local oscillator current dominates the photoinduced shot noise and find

$$\left(\frac{S}{N}\right)_H = \frac{\eta P_S}{h\nu B}\left\{1 + \frac{I_D}{I_{L.O.}} + \frac{2k(T+T')}{I_{LO} R_D}\ (1 + R_S (G_D + \omega^2 C^2 R_S))\right\}^{-1}. \tag{15}$$

For much of our discussion, we will consider a normalized signal-to-noise ratio, $(S/N)_N$, defined as the reciprocal of the bracketed quantity. If the local oscillator power is sufficiently large so that $I_{LO} \gg I_D$ and shot noise dominates thermal noise, the normalized signal-to-noise ratio approaches unity. Even in this limit, the quantum noise limit, the normalized signal-to-noise ratio depends on temperature and bias via the quantum efficiency.

The frequency response of the diode will be considered for two cases. If shot noise dominates thermal noise at all frequencies of interest, then the signal-to-noise ratio is frequency independent; however, both a decrease in the signal and shot noise occur when

$$f = \frac{\omega}{2\pi} > \frac{1}{2\pi R_S C}\,. \tag{16a}$$

On the other hand, for thermal noise limited systems the signal-to-noise ratio decreases when

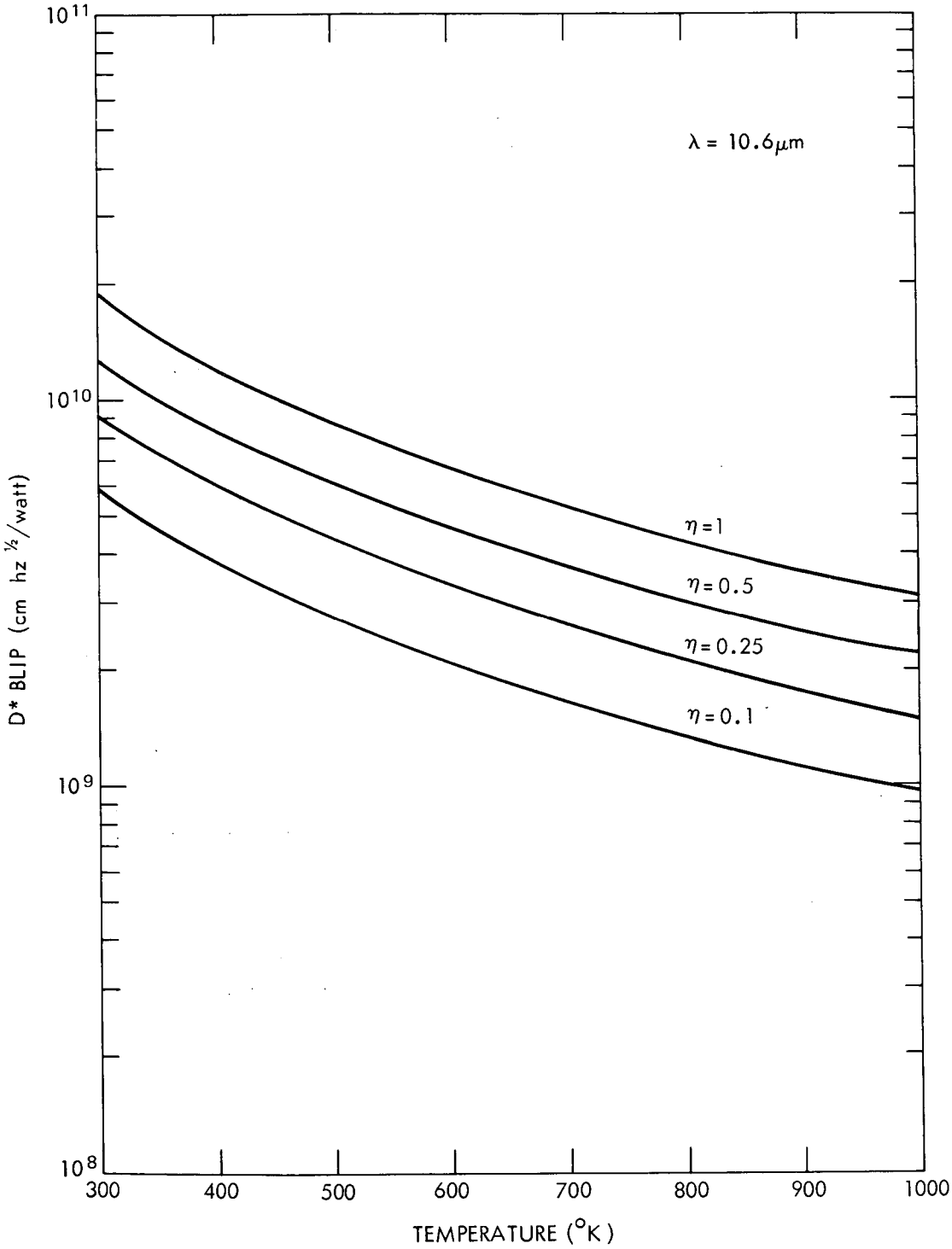

Figure 2. Background Limited Detectivity vs. Temperature

$$f > \frac{1}{2\pi\sqrt{R_D R_S C}} . \tag{16b}$$

Since as a rule $R_D > R_s$, the thermal noise limited diode has a smaller frequency response than the shot noise limited one. Unless otherwise specified, we will use equation (16a) to define the frequency response.

III. MATERIAL PARAMETERS

A. Energy Gap

The energy gap, E_g, of both HgCdTe and PbSnTe varies as a function of temperature and mole fraction of the constituent molecules. Denoting by x the mole fraction of CdTe in HgCdTe and SnTe in PbSnTe, we have the notation: $Hg_{1-x}\ Cd_x\ Te$ and $Pb_{1-x}\ Sn_x Te$. Then for $Hg_{1-x}Cd_x\ Te$[2]

$$E_g = 1.59x - .25 + 5.233 \times 10^{-4} T(1 - .208x) + .327x^3 \tag{17}$$

and for $Pb_{1-x}Sn_x Te$[3]

$$E_g = - .48478x + .1830 + 4.5654 \times 10^{-4} T(1 - .11x). \tag{18}$$

The energy gap is plotted as a function of temperature and x in Fig. 3. It is evident that the detector operating temperature is a critical element in determining sensitivity to a particular wavelength of light. A detector which is sensitive to 10.6 μm radiation (.117 ev.) at 100°K will not respond to the same radiation when the operating temperature is 175°K. Similarly, a detector designed for ten micron detection at 175°K will be less sensitive to this radiation at 100°K, rather it will be sensitive to longer wavelengths. For a 100°K detector the suitable concentration of CdTe is about 19.6% and of SnTe about 28%; at 175°K, the CdTe concentration should be about 18.6% while that of SnTe should be about 30%.

The dependence of energy gap on temperature changes is readily found to be

$$\frac{dE_g}{dT}(HgCdTe) = 5.233 \times 10^{-4} (1 - .208x) \tag{19}$$

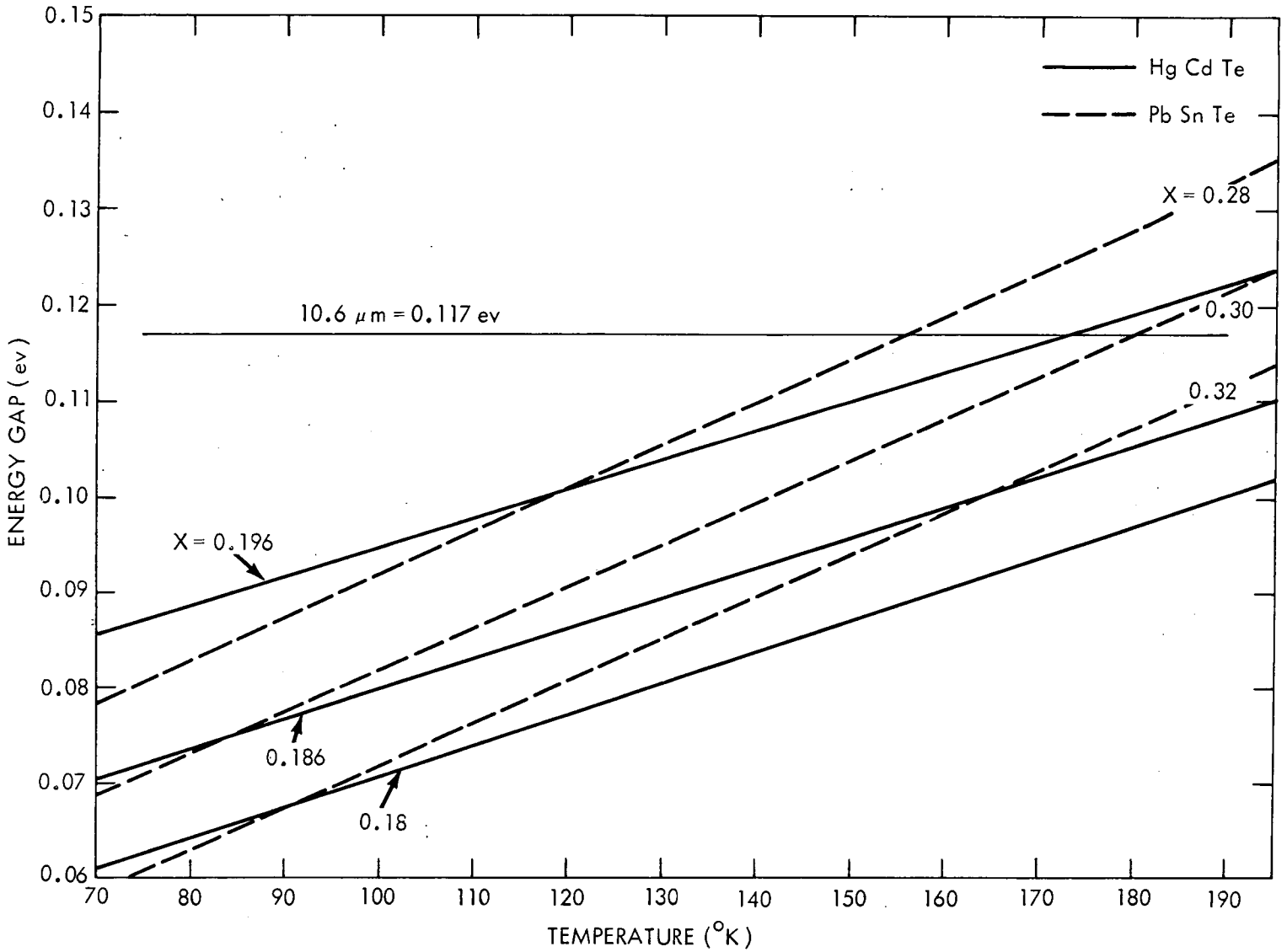

Figure 3. Energy Gap vs. Temperature for Hg_{1-x} Cd_x Te and $Pb_{1-x}Sn_x$ Te

and

$$\frac{dE_g}{dT}\,(PbSnTe) = 4.565 \times 10^{-4}\,(1 - .11x). \tag{20}$$

The sensitivity to variations in crystal composition, x, is also readily computed

$$\frac{dE_g}{dx}\,(PbSnTe) = -.48 - 5.1 \times 10^{-5}\,T. \tag{21}$$

and

$$\frac{dE_g}{dx}\,(HgCdTe) = 1.59 - 1.09 \times 10^{-4}\,T + .971x^2 \tag{22}$$

From these expressions, we conclude that the two materials have similar sensitivity to temperature changes and that PbSnTe is three to four times less sensitive to non-uniformities in crystal composition. This latter point is of some significance since crystal growth often leads to both composition irregularities and gradients.

B. Charge Carrier Concentration

Calculations of thermal equilibrium charge carrier density, n_i, can be performed both in the context of the classical parabolic energy band approximation and in the k·p approximation for small energy gap semiconductors. Provided the effective mass is allowed to vary with temperature, the two calculations yield essentially the same results[4]. The dependence of intrinsic carrier density of HgCdTe on temperature is shown in Figs. 4 and 5. In order to compare the densities for HgCdTe and PbSnTe, we use the parabolic approximation for n_i

$$n_i = \left(\frac{2\pi kT}{h^2}\right)^{3/2} (m_e\, m_n)^{3/4} \exp(-Eg/kT) \tag{23}$$

where m_e and m_h are the electron and hole density of state effective masses. Denoting the free electron mass by m_o and using the representative values:

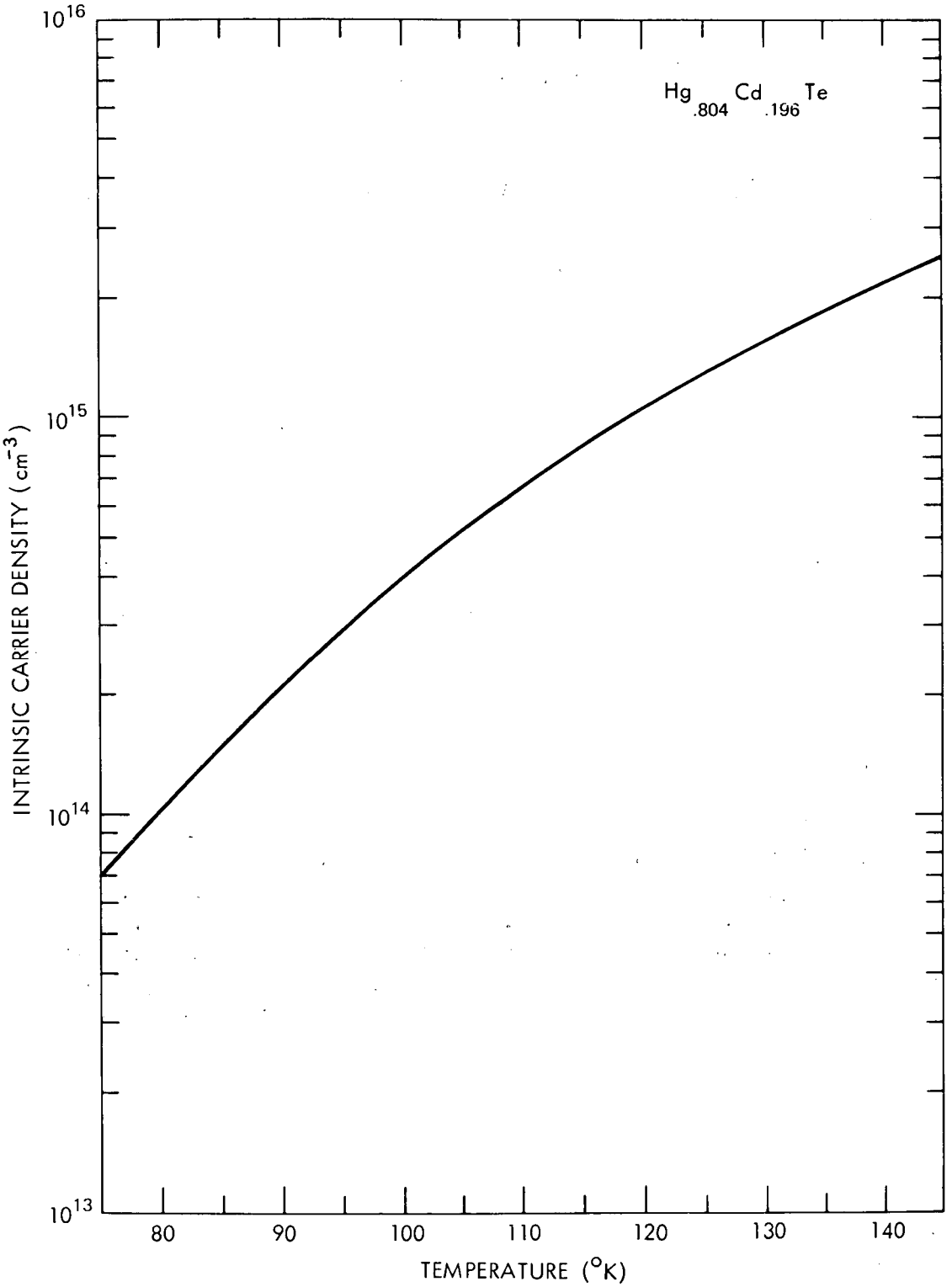

Figure 4. Temperature Dependence of Intrinsic Carrier Density for Low Temperature Detector

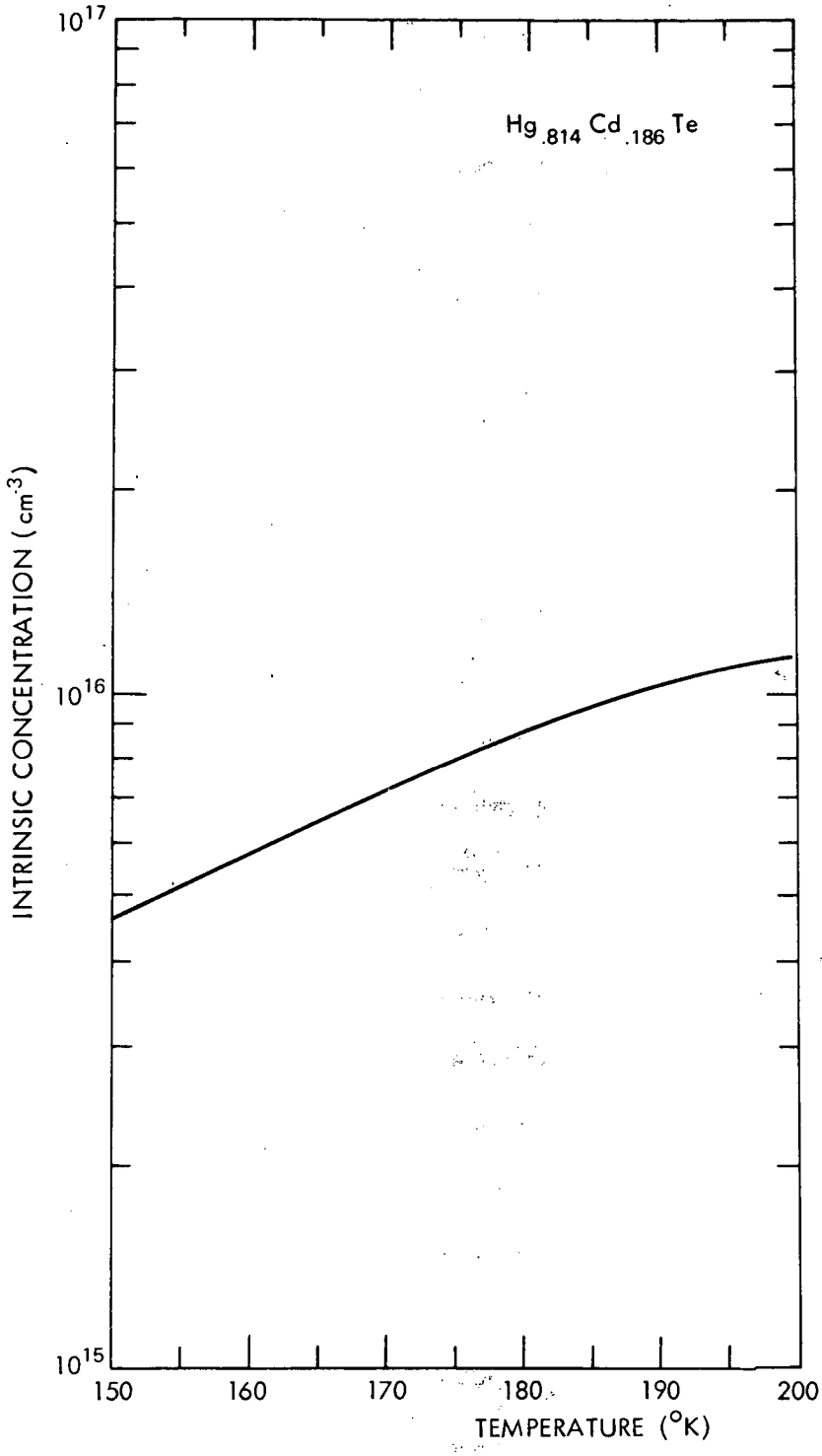

Figure 5. Temperature Dependence of Intrinsic Carrier Density for High Temperature Detector

$$\text{Hg Cd Te:}\quad \frac{m_e}{m_0} = .008;\ \frac{m_h}{m_0} = .3$$

$$\text{Pb Sn Te:}\quad \frac{m_e}{m_0} = \frac{m_h}{m_0} = .07$$

we find

$$\frac{n_i\ (\text{Hg Cd Te})}{n_i\ (\text{Pb Sn Te})} \approx .6 \tag{24}$$

for materials with the same energy gap. From this it follows that the impurity doping levels required to achieve diode characteristics are comparable for the two materials. At 100°K less than 10^{16} impurity atoms/cubic centimeter are required; while at 175°K 10^{17} impurity atoms/cubic centimeter are required. This has significant implications for device resistance and frequency response as we will show later.

The small value of the electron effective mass in HgCdTe suggests that very few charge carriers are required to fill those portions of the conduction band near the minimum. This filling of low lying levels, the Burstein-Moss effect, may be caused by photogenerated carriers as well as thermally excited ones. It leads to an effective band gap greater than those indicated by Figure 3. The x values quoted earlier for optimal 100°K and 175°K operation reflect an estimate of this band filling.

C. Absorption Coefficient and Quantum Efficiency

An approximate value for the absorption coefficient, x, can be calculated from the relation[5]

$$\alpha = \frac{(2m_r)^{3/2}\ e^2\ (Eg - h\nu)^{1/2}}{n\ h^2\ cm_e\ \epsilon_0} \tag{25}$$

where $m_r = m_e m_h/(m_e + m_h)$ is the electron-hole reduced mass, n is the index of refraction, c the space of light and ϵ_0 the permitivity of free space. For $n_{HgCdTe} = 4$, $n_{PbSnTe} = 7$ and effective masses as before

$$\frac{\alpha\,(\mathrm{Hg\ Cd\ Te})}{\alpha\,(\mathrm{Pb\ Sn\ Te})} \approx 1.6 \tag{26}$$

indicating that the absorption coefficients of the two materials are comparable. While the calculation above suggests that α(HgCdTe) > α(PbSnTe), data indicates that at 77°K α(HgCdTe) $\sim 10^3\ \mathrm{cm}^{-1}$ while α(PbSnTe) $\sim 10^4\ \mathrm{cm}^{-1}$.[6,7] The reason for this discrepancy is not known. In any case, junction depths of 1 to 10 micrometers are required to assure radiation being absorbed before the junction.

The quantum efficiency of the photodiode is the ratio of the number of photo-excited charge carriers reaching the junction to the number of incident photons and is a function of the absorption coefficient and diffusion length of the carriers. Melngailis and Harman[8] present an expression for quantum efficiency based on the assumption that all absorption takes place at the detector surface, i.e. $\alpha \to \infty$. They find

$$\eta = \frac{1 - R}{\cosh\frac{d}{L} + \frac{v\tau}{L}\sinh\frac{d}{L}} \tag{27}$$

where R is the reflection coefficient related to the index of refraction by

$$R = \left(\frac{n - 1}{n + 1}\right)^2,$$

d is the junction depth, L is the minority carrier diffusion length, v, is the surface recombination rate, and τ is the minority carrier bulk lifetime. For small surface recombination

$$\eta = \frac{1 - R}{\cosh\frac{d}{L}}. \tag{28}$$

The effect of a finite absorption coefficient is to decrease the excitations at the surface while allowing for possibility of charge carrier generation within the bulk. At a distance x from the surface of the diode, the ratio of number of photons unabsorbed to the number incident on the detector front surface, r, is

$$r = e^{-\alpha x} \tag{29}$$

If for all x, y < L, then we can estimate η from

$$\eta = \frac{(1 - R)\,(1 - e^{-\alpha d})}{\cosh \frac{d}{L}}, \tag{30}$$

For a high quantum efficiency $L > d > 1/\alpha$, but these conditions cannot always be simultaneously satisfied. For example, with a mobility, μ, of 10^4 cm^2/volt-sec a bulk minority lifetime of 10^{-8} sec at a temperature of 100°K

$$L = \left(\frac{k T \mu}{e}\right)^{1/2} = 9.3\ \mu m \tag{31}$$

This implies that a junction depth of not more than a few micrometers is required to assure that all carriers diffuse to the junction before recombining. However, with $d = 3\ \mu$m and $\alpha = 1000$ cm^{-1} then $\alpha d = 3$, which fails to satisfy the condition $\alpha d > 1$. The quantum efficiency decreases with increasing temperature as Fig. 6 illustrates. This is primarily due to the increase in the width of the energy gap (which causes the absorption coefficient to decrease). A secondary effect is a decrease in diffusion length at high temperatures due to decreased carrier mobility.

D. Frequency Response

The frequency response of a photodiode can be limited by carrier transit times or electrical circuit constraints. If a carrier is generated a distance s from the junction, it diffuses to the junction in a mean time

$$T_r = e\, s^2 / k T \mu. \tag{32}$$

For a distance, s, of 3μ m and a mobility of 10^5 cm^2/volt sec at 77°K, the diffusion time is 0.10 nanoseconds (nsec) while with the same s and a mobility of 10^4cm^2/volt sec at T = 150° the transit time is .11 nsec, indicating a slight degradation in the diffusion time at the higher temperature. The 0.10 nsec is equivalent to a frequency response of 1.6 gigahertz while .11 nsec is equivalent

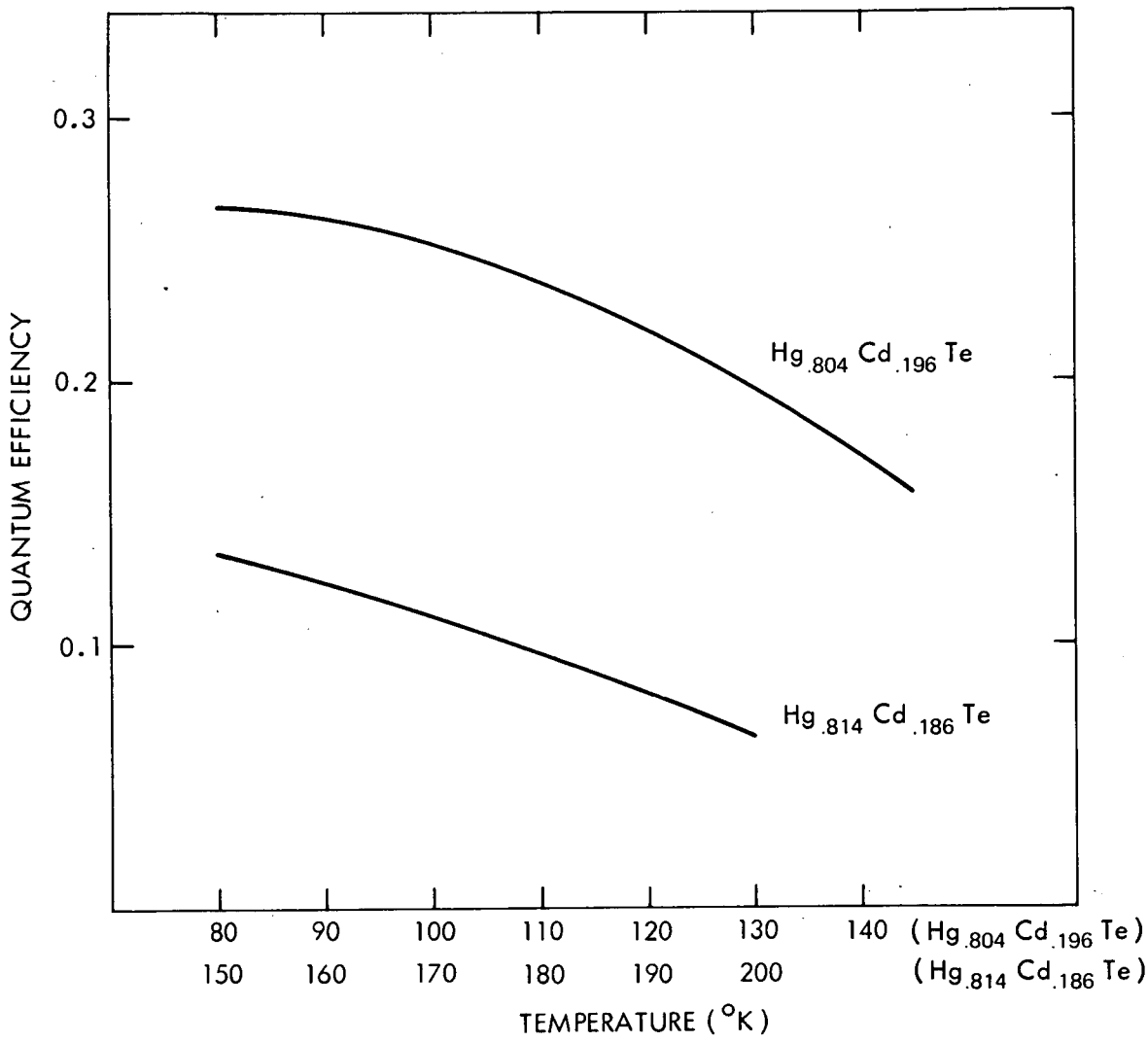

Figure 6. Temperature Dependence of Quantum Efficiency

to 1.4 gigahertz. The greater electron mobility in HgCdTe as opposed to that in PbSnTe (Section IIF) gives the former material an advantage in overcoming diffusion time limitations.

A more critical limitation on the response time is imposed by resistance capacitance effects. As Eq. 15 shows device performance is degraded at all frequencies such that

$$f > \frac{1}{2\pi R_s C}. \tag{33}$$

The capacitance is a function of applied voltage, the impurity profile, (spatial distribution), and the dielectric constant of the material. For an abrupt transition between the p and n regions of the diode

$$C = \left(\frac{\epsilon N_D N_A}{e (N_D + N_A) (- V)} \right)^{1/2} \tag{34}$$

where ϵ is the dielectric constant on the material, N_D and N_A the donor and accepter concentrations and V the bias. In practice, the capacitance has been found to vary typically from the inverse one-third power to inverse unity power of the voltage. We note that the increased carrier concentrations required by high temperature diodes increase the capacitance. The dependence of the R-C bandwidth on voltage is shown in Fig. 7. It should be mentioned that because the dielectric constant of PbSnTe ($\sim$200) is much greater than that of HgCdTe ($\sim$16); the R-C limitations on PbSnTe are more severe than on HgCdTe.

E. Minority Carrier Bulk Lifetime

The minority carrier bulk lifetime is required to estimate the diffusion length of the carriers. Beside recombination through surface states, electrons and holes can recombine in the bulk via both radiative and non-radiative processes. Direct radiative recombination of electrons and holes with the emission of photon is characterized by a lifetime, τ_{DR},

$$\tau_{DR} = \frac{n_i^2}{Gr (n_0 + p_0 + \Delta n)} \tag{35}$$

where n_0 and p_0 are the thermal equilibrium densities of electrons and holes in any one side of the device, Δn is the density of photogenerated pairs in that region and

$$Gr = 8\pi \frac{n}{c} \int_{Eg/h}^{\infty} \frac{\alpha (v)\, dv}{e^{\nu/kT} - 1}. \tag{36}$$

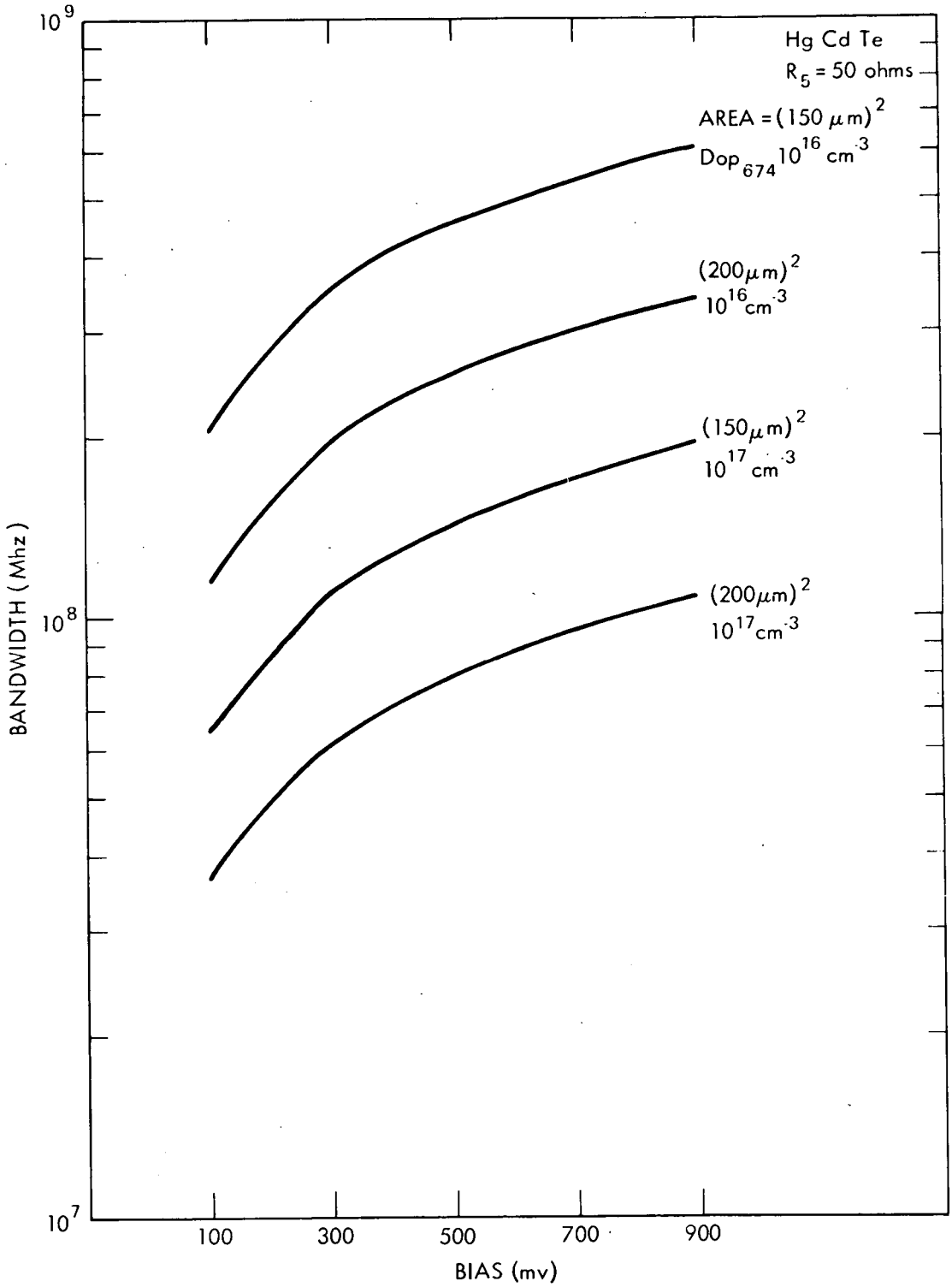

Figure 7. Frequency Response of Diode

Using Eq. 25 for α and assuming $E_g/kT >> 1$, the integral can be evaluated with the same result

$$Gr = \frac{8\pi^{3/2} e^2 n (kT)^{5/2} (2 m_r)^{3/2}}{c^3 h^5 m_e \epsilon_0} \left\{\frac{15}{8} + \frac{3}{2}\frac{Eg}{kT} + \frac{1}{2}\left(\frac{Eg}{kT}\right)^2\right\} \exp\left\{-\frac{Eg}{kT}\right\} \quad (37)$$

In practice, $N_D \sim n_0 >> p_0$ (or $N_A \sim p_0 >> n_0$) where N_D (N_A) is the density of donor (acceptor) atoms on the n(p) side of the junction.

In the non-radiative Auger process, the minority carrier lifetime is

$$\tau_A = \frac{2 n_i^2 \tau_i}{(n_0 + p_0 + \Delta n)(n_0 + \Delta n + \beta (p_0 + \Delta n))} \quad (38)$$

where

$$\tau_i = \frac{3.8 \times 10^{-18} \left(\frac{\epsilon}{\epsilon_0}\right)^2 (1 + U)(1 + 2U) \exp\left(\frac{1 + 2U}{1 + U}\frac{Eg}{kT}\right)}{\frac{m_e}{m_0} |F_1 F_2|^2 \left(\frac{kT}{Eg}\right)^{3/2}} \quad (39)$$

and

$$U = \frac{m_e}{m_h} .$$

Here F_1 and F_2 are the overlap integrals of the periodic parts of the Bloch functions for the two bands. We have used the value $|F_1 F_2| = .165$ in our calculations.[9] Eq. (38) is derived under the assumption of parabolic bands. Peterson[10] has derived a corresponding expression in the k·p formulation; however, the lifetimes calculated from the two expressions do not differ significantly.

Carrier recombination through flaw levels and traps is important particularly in PbSnTe and also in HgCdTe at temperatures below 100°K. The Shockley-Read model for recombination through a set of monovalent flaws yields a lifetime

$$\tau_{SR} = \frac{\tau_{n0}(p_0 + p_1 + \Delta n) + \tau_{p0}(n_0 + n_1 + \Delta n)}{n_0 + p_0 + \Delta n} . \quad (40)$$

The quantities τ_{n0} and τ_{p0} are constants and p_1 and n_1 are the electron and hole densities when the Fermi level is at the recombination flaw energy. In the context of a general discussion, one must consider the variation of carrier lifetimes with the number of photoexcited carrier, Δn. For small volume photoconductors, the expressions used above must be modified to take into account the rate of change of carrier recombination with increasing radiation intensity. The criterion for such modification is that the number of photoexcited carriers become comparable to the number of majority carriers in thermal equilibrium. If θ is the number of photons/sec., illuminating the photodetector, then the number of photoexcited carriers is $\eta\theta$. For a quantum efficiency of 20% and a power of 10^{-3} watts at 10.6 μm, about 10^{16} carriers/second are generated. If the device is a high speed detector, then the minority carriers transit from the surface to the junction in about 10^{-10} sec., so about 10^6 minority carriers are present in the steady state. For a small volume detector ($\sim 5 \times 10^{-7}$ cm^3), there may be 10^9 majority carriers on each side of the junction but only 10^3 minority carriers in thermal equilibrium. We conclude that the lifetime of the minority carriers in the photodiode is not appreciably altered by the illumination. Note, however, that the density of minority carriers; hence, the reverse bias current is appreciably altered.

The net lifetime is formed from the reciprocal addition of the individual lifetimes. Figure 8 shows representative temperature variation of the hole lifetime in n-type HgCdTe. Auger recombination dominates the lifetime of heavily doped n-type HgCdTe and the Shockley-Read recombination dominates in both n-type and p-type PbSnTe. The lifetime mechanism for p-type HgCdTe, as determined by the experiment, is about 10^{-9} seconds. This cannot be explained by the mechanisms discussed here, although the presence of high density of impurities in the measured samples suggests that recombination through flaw or impurity levels should be important.

F. Charge Carrier Mobility

The mobility of charge carriers is important in the determination of carrier diffusion times, diode resistance, and quantum efficiency; a high mobility is required to assure that all photogenerated charge carriers reach the junction. The mobility is limited by scattering due to lattice vibrations, impurities, or other crystal imperfections. The measured electron mobility in HgCdTe is 10^5 cm^2/volt-sec and that of the holes 10^4 cm^2/volt-sec at 100°K. In PbSnTe both the electrons and holes have mobilities of 2.5×10^4 cm^2/volt-sec at 100°K. An implication of these numbers is that high speed, high sensitivity HgCdTe photodiodes must use the electrons as the minority carriers in the photoactive region, whereas the choice between electrons and holes in PbSnTe is independent of these considerations. This point weighs somewhat in favor of PbSnTe since

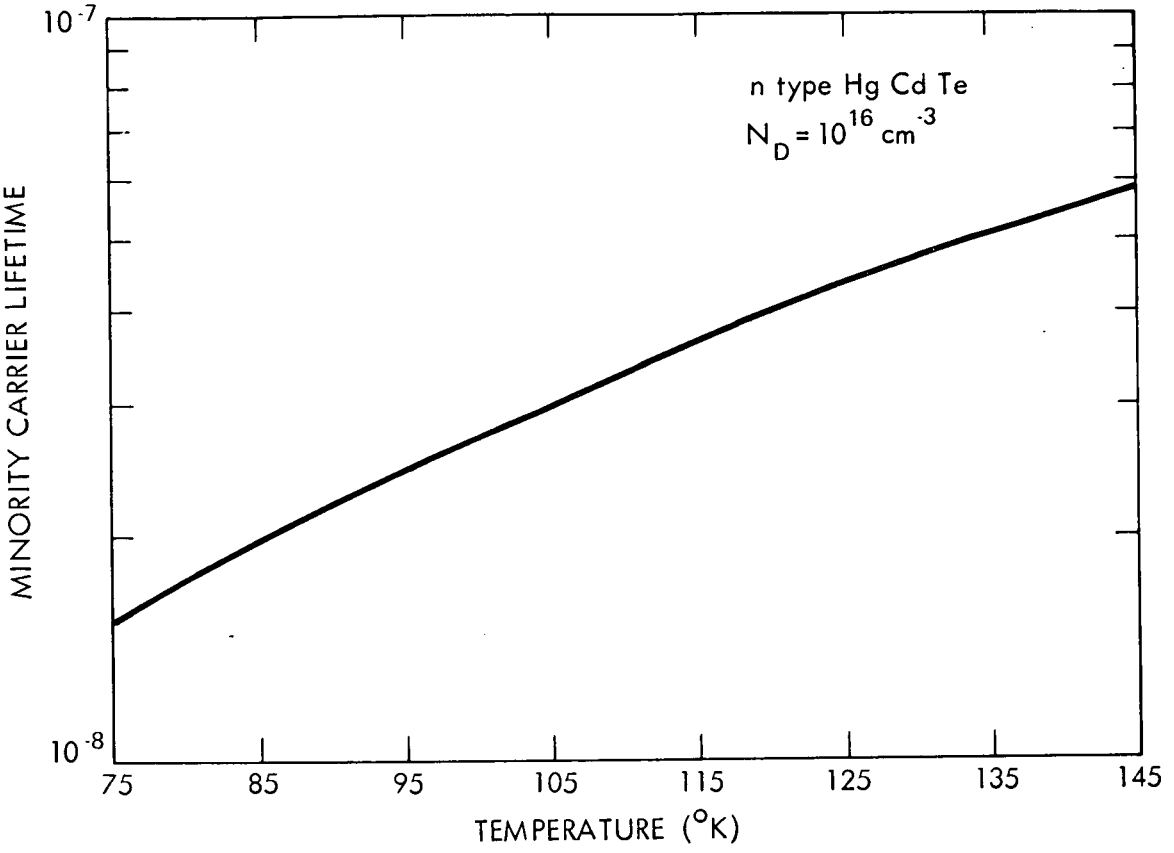

Figure 8. Hole Lifetime in n Type Hg Cd Te

p on n diodes in HgCdTe have been difficult to fabricate. Another implication is that PbSnTe diodes must be fabricated with a more shallow junction than HgCdTe to maintain the same transit time characteristics. This implies a reduction in quantum efficiency for PbSnTe since the product αd is reduced. The reduction is mitigated somewhat by the fact that minority carriers from both sides of junction may contribute to signal detection in PbSnTe. On the other hand, the temperature dependence of the mobilities, $T^{-1.5}$ for HgCdTe and $T^{-2.5}$ for PbSnTe indicates more severe degradation in the current carrying capabilities of PbSnTe than HgCdTe at elevated temperatures. Coupled to the factor of 4 greater electron mobility in HgCdTe than in PbSnTe at 100°K, the mobility of electrons in PbSnTe is only 1/6 that in HgCdTe at 150°K. The temperature variation of the electron mobilities at temperatures less than 150°K is shown in Fig. 9.

G. Current-Voltage Characteristics and Junction Resistance

The current-voltage characteristics of a diode depend on the concentration of the dopant atoms, the temperature, the mobility of the charge carrier, the

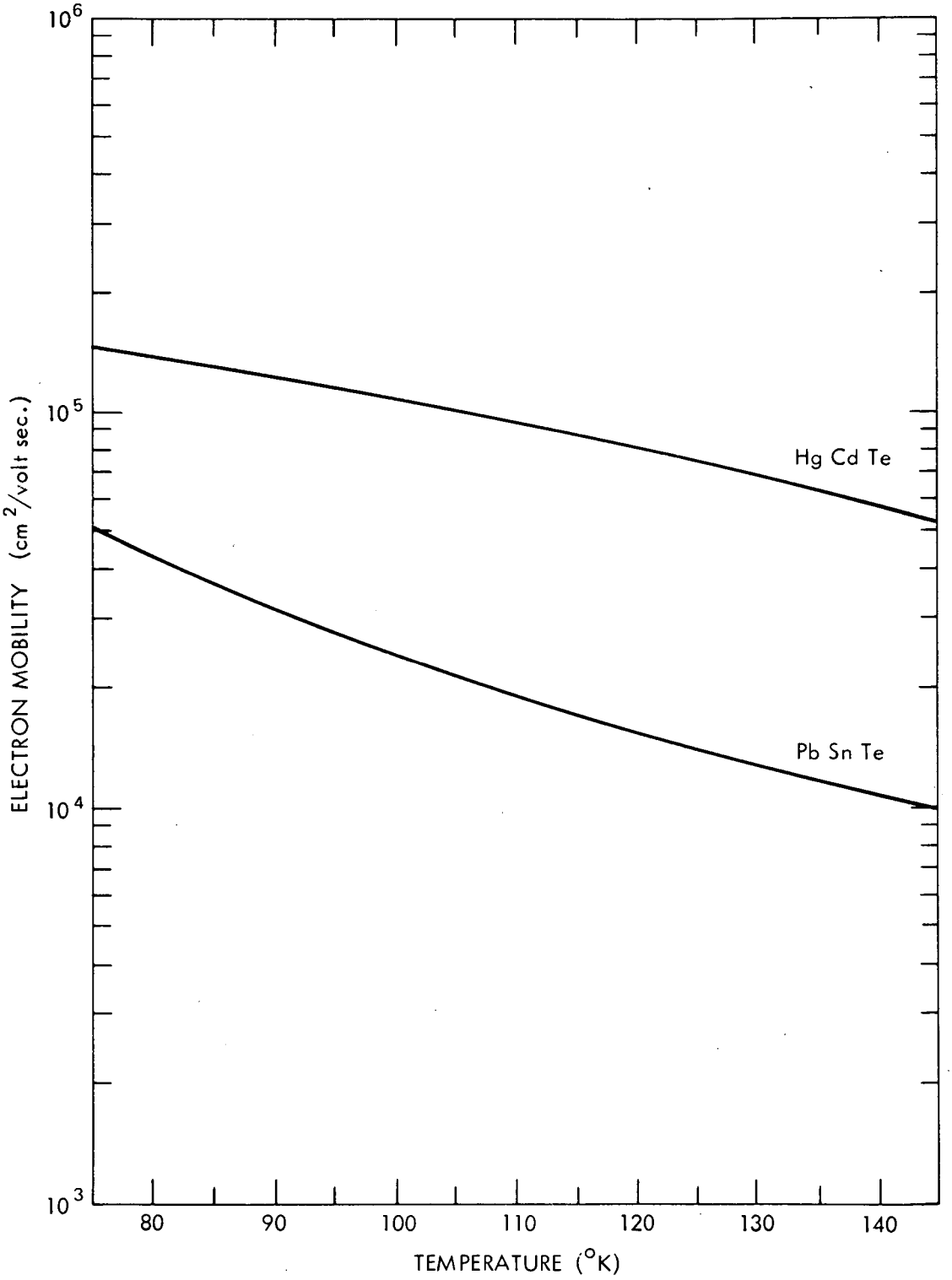

Figure 9. Temperature Dependence of Electron Mobility

intrinsic carrier concentration, and the diffusion length for the carriers. Ideally for a shallow junction p-n device, the current is

$$I = I_{sat} \left(e^{eV/KT} - 1\right) \tag{41}$$

where the saturation current, I_{sat}, is

$$I_{sat} = A\, n_i^2 \left(\frac{kT\,\mu_e}{N_D d} + \frac{kT\,\mu_h}{N_A L_h}\right) \tag{42}$$

As before the subscripts e and h are used to designate electron and hole respectively. When the diode is illuminated the saturation current contains another component

$$I'_{sat}(P) = \frac{e\,\eta P}{h\,\nu}$$

where P is the power of the illuminating beam striking the detector surface. The variation of saturation current with temperature is shown in Fig. 10. Due to leakage across the junction, we must add to this a bias dependent term, I_v, which we assume takes the form $|I_v| = G_L V$. The leakage conductance, G_L, typically takes a value of 100 - 500 in HgCdTe for 77°K < T < 150°K. For $|V| > kT/e$

$$-I = I_{sat} + G_L V \tag{42}$$

With a bias of .5 volts, $I_v \sim 1$ ma. At 100°K, this is typically a factor of 10 greater than the saturation current indicating leakage current dominates the I-V characteristics. Because high temperature photodiodes require increased doping levels beyond those required at 100°K, we expect that both I_s and I_v are also greater in high temperature diodes. We will conjecture for this analysis the leakage current is due to conduction by the majority carriers and is proportional to the majority carrier mobility and concentration accordingly.

$$\frac{I_L(150\,°K)}{I_L(100\,°K)} = \frac{N_D(\text{required at } 150\,°K)}{N_A(\text{required at } 100\,°K)}\,\frac{\mu(150\,°K)}{\mu(100\,°K)} \approx 7 \tag{43}$$

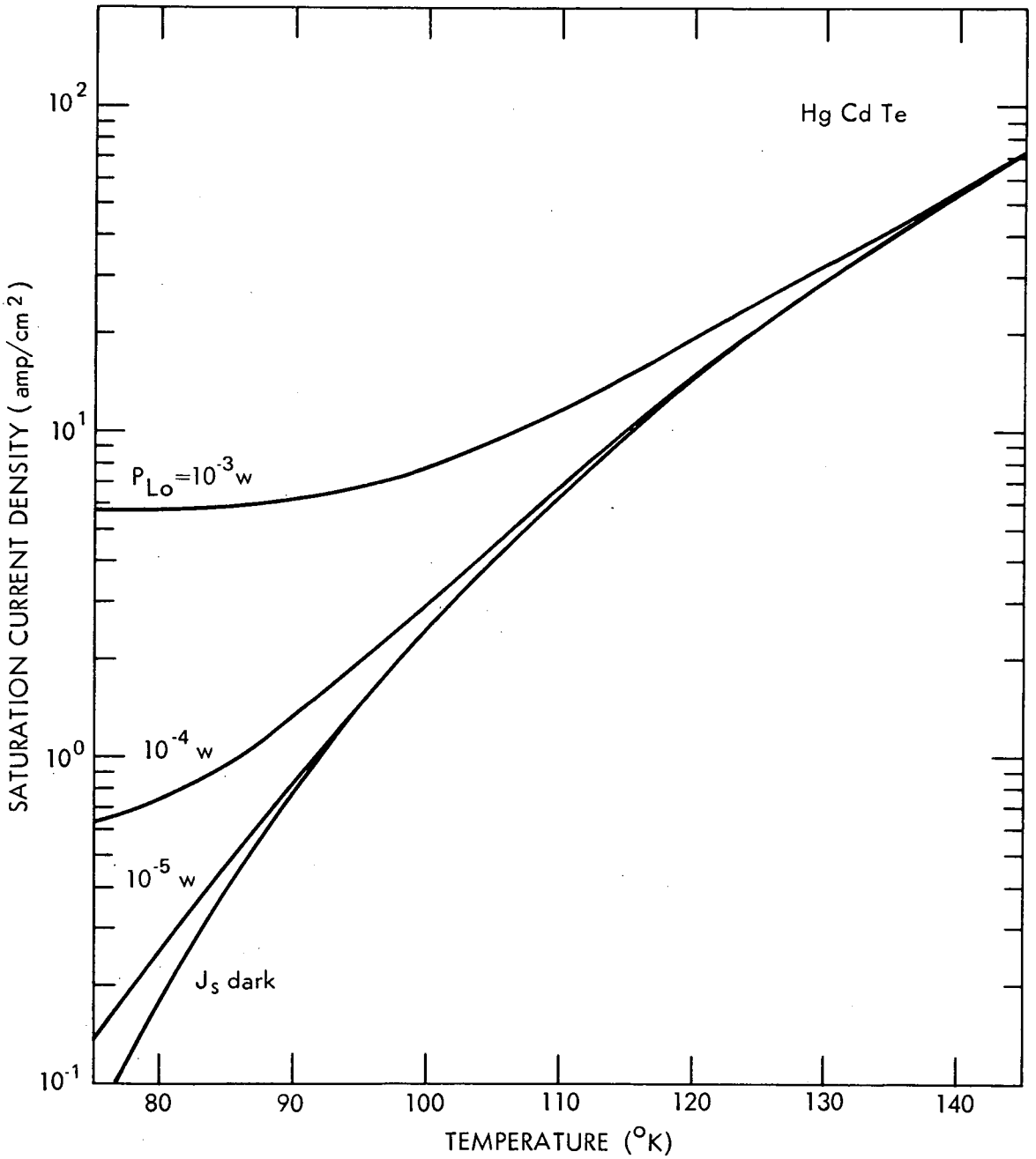

Figure 10. Ideal Diode Current vs. Temperature

so that ~10 milliamps of dark current may be expected at 150°K. This high value of the dark current at elevated temperature has two very detrimental effects on device performance. It increases the dark current contribution to the shot noise, necessitating the use of more than ten milliamps of photocurrent to overcome the dark current. It also increases the power the diode must dissipate.

This latter point is particularly critical. If V~ 1 volt, then the diode must dissipate > 10 milliwatts to maintain the desired operating temperature. In a moment, we will see that this may not be possible. However, if leakage current can be overcome, PbSnTe is less likely to heat than HgCdTe because of its smaller dark current.* Summarizing these remarks: The increased diode current in a high temperature device caused by the increased saturation current and increased leakage current require that more than ten milliwatts of photocurrent be generated to assure that photocurrent dominates the shot noise. The increased current increases the power that must be dissipated causing a potential heating problem in the diode.

H. Power Dissipation by Diode

In this section, we estimate the effect of the thermal conductivity on the power dissipation at 150°K. Heat flow from the diode to a cold shield can be limited by the diode material, the epoxy used to hold the diode, or the substrate material. In order to achieve the highest possible thermal and electrical conductivity, the diode may be epoxied directly to the cold finger with gold (or other suitable conducting metal) impregnated epoxy. For at least one gold impregnated epoxy, the thermal conductivity, K, at 290°K ~ one-tenth that of gold.[11] We assume therefore

$$K_{epoxy} = .03 \left(\frac{290}{T}\right)^{1.5} \frac{watts}{cm\ ^{\circ}K} . \tag{44}$$

The thermal conductivity of heavily doped HgTe is .15 (77/T) watts/cm °K while that of CdTe is .4 $(77/T)^{1.3}$ watts/cm °K . We then find that at 150°K

$$\begin{aligned} K_{HgTe} &= .08 \\ K_{CdTe} &= .17 \\ K_{epoxy} &= .08 . \end{aligned} \tag{45}$$

Since the epoxy layer is more than an order of magnitude thinner than the detector, thermal conductance is limited by the detector material not the epoxy. If the thermal conductivity of the compound Hg_{1-x} CdTe is proportional to the fractional content of the constituent molecules then for

*Due to smaller carrier mobility

$$Hg_{.82}\,Cd_{.18}\,Te \text{ at } 150°,\ K = .09\frac{watt}{Cm\,°K}\ .$$

Now since

$$\frac{P_t}{A} = \frac{K\Delta T}{\ell} \tag{46}$$

where P_t is the power that must be dissipated through an area A and a length ℓ, we find

$$\Delta T = 83.3\ P_T \tag{47}$$

for $A = 4 \times 10^{-4}$ cm^2 and $\ell = 30$ μm. In Table I, we tabulate ΔT for several values of P_t. In view of our earlier observation that 10 - 100 milliwatts may need to be dissipated at 150°K, it is clear that heating of the diode can occur at this temperature.

IV. SIGNAL-TO-NOISE RATIO, RESULTS OF CALCULATION

In Section II, we indicated that the performance of a photodiode depends on its quantum efficiency, resistance, ratio of dark current to photocurrent, and capacitance. In Section III, we related these quantities to the energy gap, carrier concentration, effective mass, absorption coefficient, diffusion length, mobility, lifetime, and junction depth. We indicated in that section how these intrinsic parameters of the detector vary with extrinsic parameters such as temperature, bias, and local oscillator power. It is evident that the signal-to-noise ratio is a complicated function of these extrinsic parameters. Accordingly, a computer program has been written to evaluate diode performance for a variety of external conditions. The inputs to the program are the mole fraction of the constituent molecules, detector size, doping concentrations, series resistance and amplifier temperature. The program calculates energy gap, intrinsic carrier concentration, carrier mobility, junction resistance, quantum efficiency, capacitance, frequency response, signal and noise currents, detectivity and other parameters. These parameters are printed out as functions of temperature, bias, and local oscillator power. There is some variation in program size depending on exact information requested, but a typical program contains 125 executable Fortran statements and can be run on an IBM 360/91 computer in less than 4 seconds of central processing unit time. Table II indicates some of

Table I

Heating of Diode at High Temperature

ℓ	A	P_T	ΔT
3×10^{-3} cm	1×10^{-4} cm^2	1 mw	0.3°K
		5	1.7
		10	3.3
		20	6.7
3×10^{-3} cm	2.25×10^{-4} cm^2	1 mw	0.1°K
		5	0.7
		10	1.5
		20	3.0
	4×10^{-4} cm^2	1 mw	0.1°K
		5	0.4
		10	0.8
		20	1.7
4×10^{-3} cm	1×10^{-4} cm^2	1 mw	0.4°K
		5	2.2
		10	4.4
		20	8.9
	2.25×10^{-4} cm^2	1 mw	0.2°K
		5	1.0
		10	2.0
		20	4.0
	4×10^{-4} cm^2	1 mw	0.1°K
		5	0.6
		10	1.1
		20	2.2

Table II

Computer Program Parameters

Parameter	Valve
Detector Area, A	4×10^{-4} cm^2
Junction Depth, d	10 μm
Amplifier Temperature, T_A	168°K
Series Resistance, R_s	50 ohms
Refractive Index, n	4.0 (Hg Te) 2.6 (Cd Te) 6.0 (Pb Te) 6.6 (Sn Te)
Donor Density, N_D	10^{16} cm^{-3} (low T diode) 10^{17} cm^{-3} (high T diode)
Acceptor Density, N_A	10^{16} cm^{-3} (low T diode) 10^{17} cm^{-3} (high T diode)
Dielectric Constant, ϵ	n^2 (Hg Cd Te) 200 (Pb Sn Te)
Light Frequency	2.83×10^{13} hz
Background Temperature, T_B	300°K

the constants used in the programs whose results are reported here. In Figs. 11 through 14, we show the results of the computer calculations of $(S/N)_N$ both as a function of local oscillator power and temperature. Fig. 11 shows the usual asymptotic approach to the quantum noise limit as local oscillator power is increased until local oscillator induced shot noise dominates all other noise terms. This requires several milliwatts of local oscillator power for the temperatures shown. Fig. 12 shows a degradation in $(S/N)_N$ as temperature is increased. This primarily reflects a decreasing quantum efficiency. Two other effects are also at work; the saturation current is increasing with increasing temperature due to greater minority carrier concentration and the leakage current is decreasing due to reduction in carrier mobility. Fig. 13 is a plot of $(S/N)_N$ for a high temperature photodiode. The signal-to-noise ratio is well below unity even at the higher values of local oscillator power. This reflects the large dark currents in a high temperature device; we have already indicated that these currents may cause heating of the device. In these figures we have assumed that diode is operating at frequency within its electrical bandwidth.

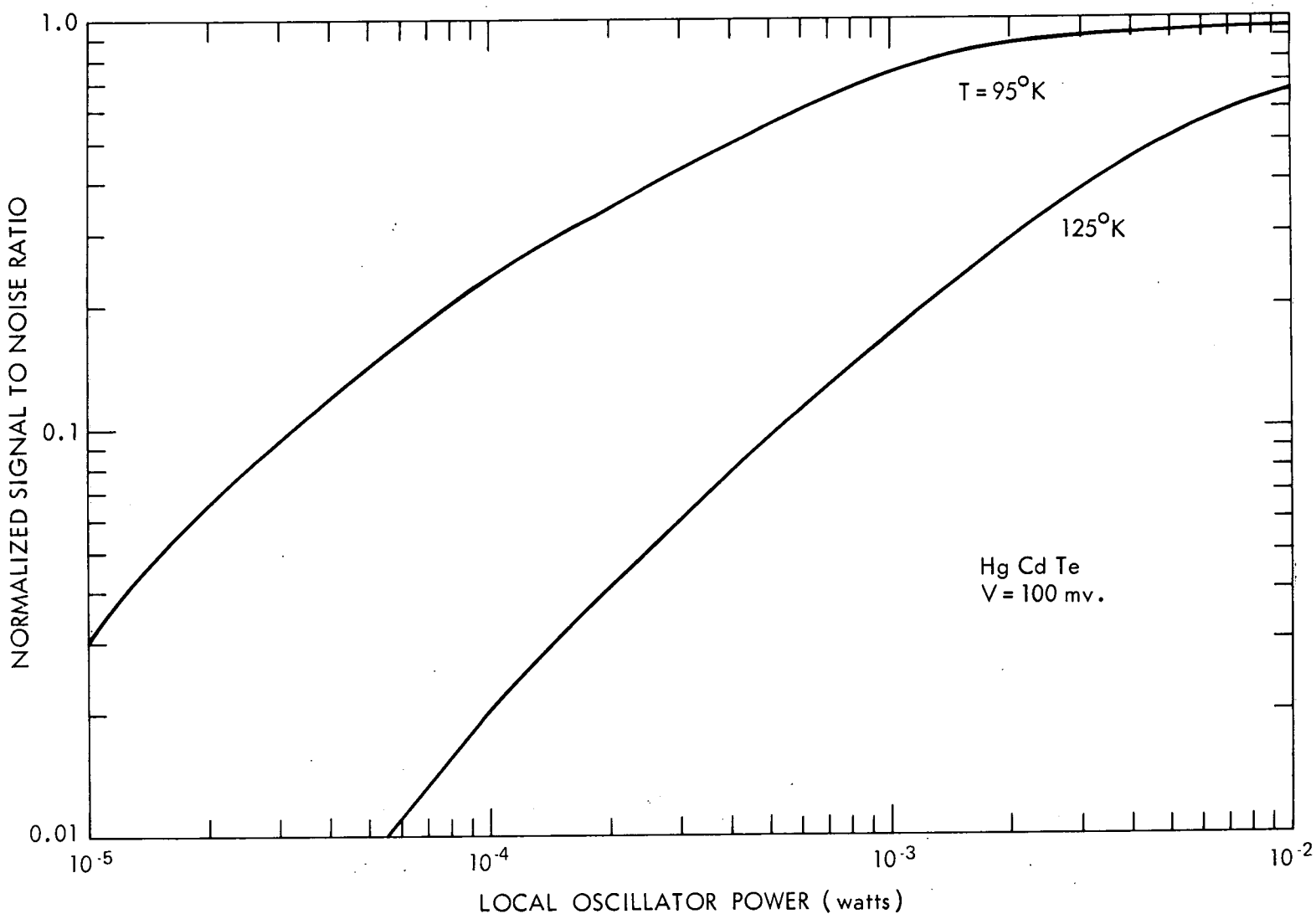

Figure 11. $(S/N)_N$ vs. Local Oscillator Power

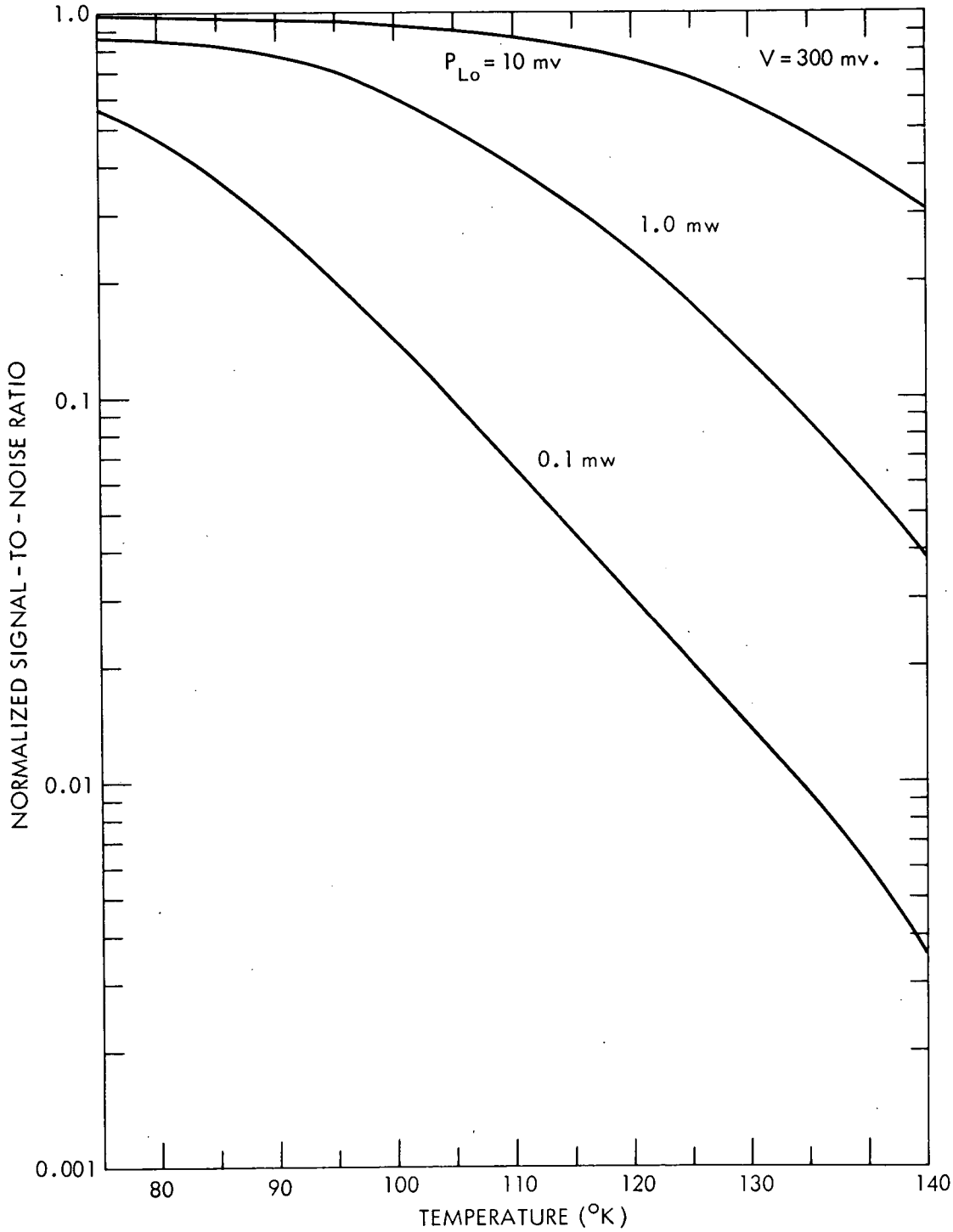

Figure 12. $(S/N)_N$ vs. Temperature (75°K–145°K)

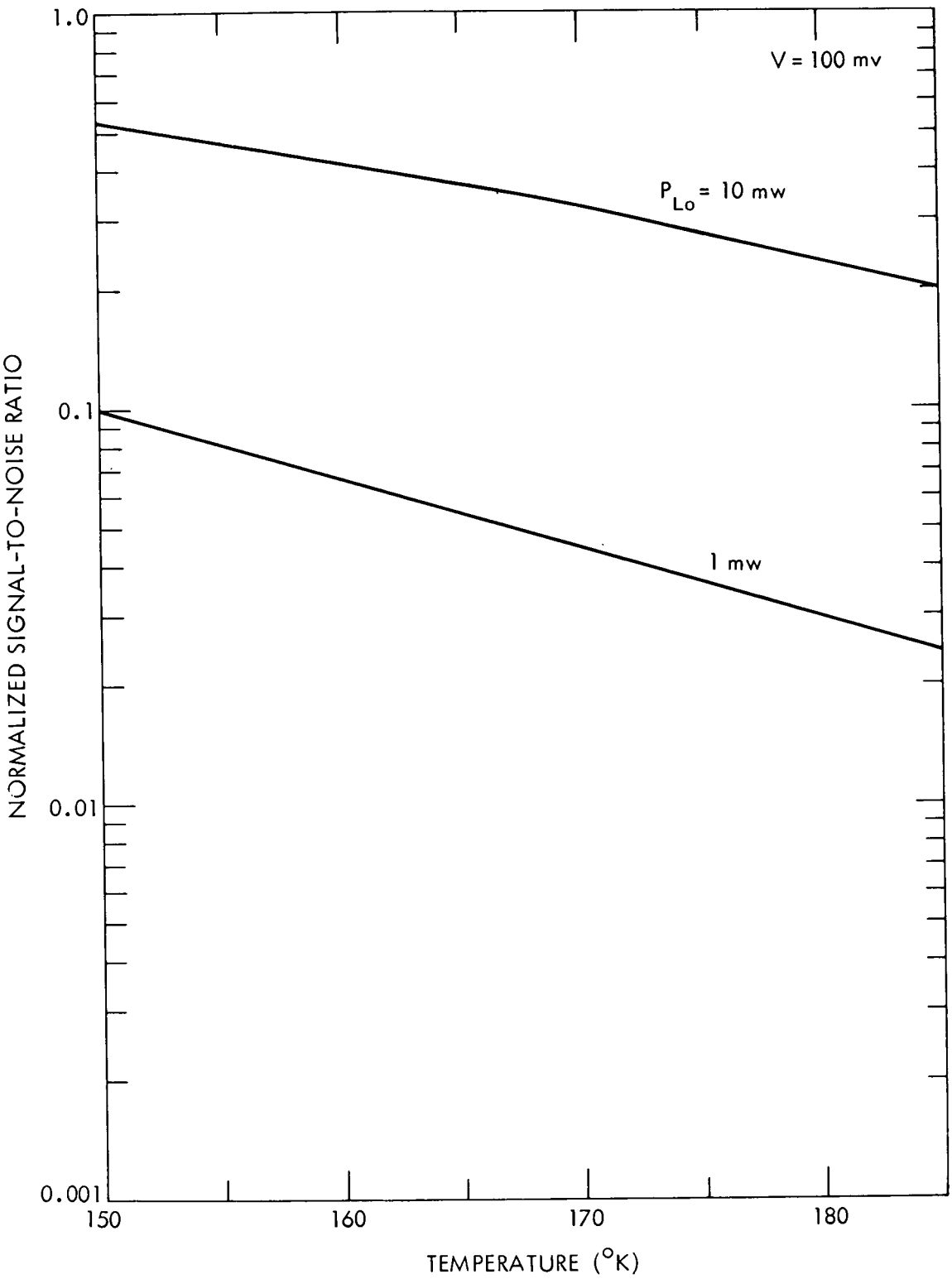

Figure 13. $(S/N)_N$ vs. Temperature (150°K–185°K)

In Fig. 14, we show the theoretical D* of a HgCdTe detector in a direct detection system with 1/f noise negligible. We have assumed that a 300°K blackbody is a source of background radiation and that the detector has a 120° field of view. Leakage current is ignored. The decreased D* as temperature is increased is due to increased saturation current and, thermal noise. The curve D^*_{Blip} is the calculated with all dark noise suppressed and indicates expected performance levels of the diode when leakage currents can be overcome, saturation current reduced and thermal noise suppressed.

It should be pointed out that the figures discussed so far in this section reflect the performance of good quality photodiodes but not ultimate limitations. Improvement in diode performance can be achieved in at least three ways. The most important of these is a reduction in the leakage currents. We have assumed a leakage conductance for both HgCdTe and PbSnTe of .002 mhoes at 77°K corresponding to a resistance of 500 ohms. Recent reports[12] indicate that reduction in leakage currents is achievable. Elimination of leakage current raises $(S/N)_N$ at 100°K and 1 mw local oscillator power from .24 to .36.

The dark current and capacitance can be considerably decreased by reducing the detector area. A decrease in the length of a square diode from 200 μm to 100 μm results in a factor of 4 decrease in the detector area and hence a factor of 4 decrease in the capacitance and minority carrier current. The result is a factor of 4 decrease in R_sC. This extends the R_sC frequency response of HgCdTe to about 1.2 GHz when R_s = 50 ohms. Finally, the quantum efficiency can be significantly improved by antireflection coating of the surface. Such coating can increase the quantum efficiency of by a factor of 1.8 in PbSnTe and 1.5 in HgCdTe.

V. SUMMARY AND CONCLUSIONS

In this section, we summarize the results of the diode analysis and formulate certain conclusions about detector performance and potential.

A. Photodiodes for Operation in the 77°K to 150°K Temperature Range

Both HgCdTe and PbSnTe can be used as quantum noise limited 10.6 μm photodiodes. The frequency response is 400 - 1200 MHz for a HgCdTe photodiode and 70 - 280 MHz for a PbSnTe photodiode when each is terminated by a 50 ohm load. Without antireflection coating, HgCdTe has a quantum efficiency of 27% at 77°K and about 15% at 150°K. Over the same range, the quantum efficiency of PbSnTe changes from 18% to less than 10%. These quantum efficiency calculations assume junction depths of 10 μm. The internal quantum

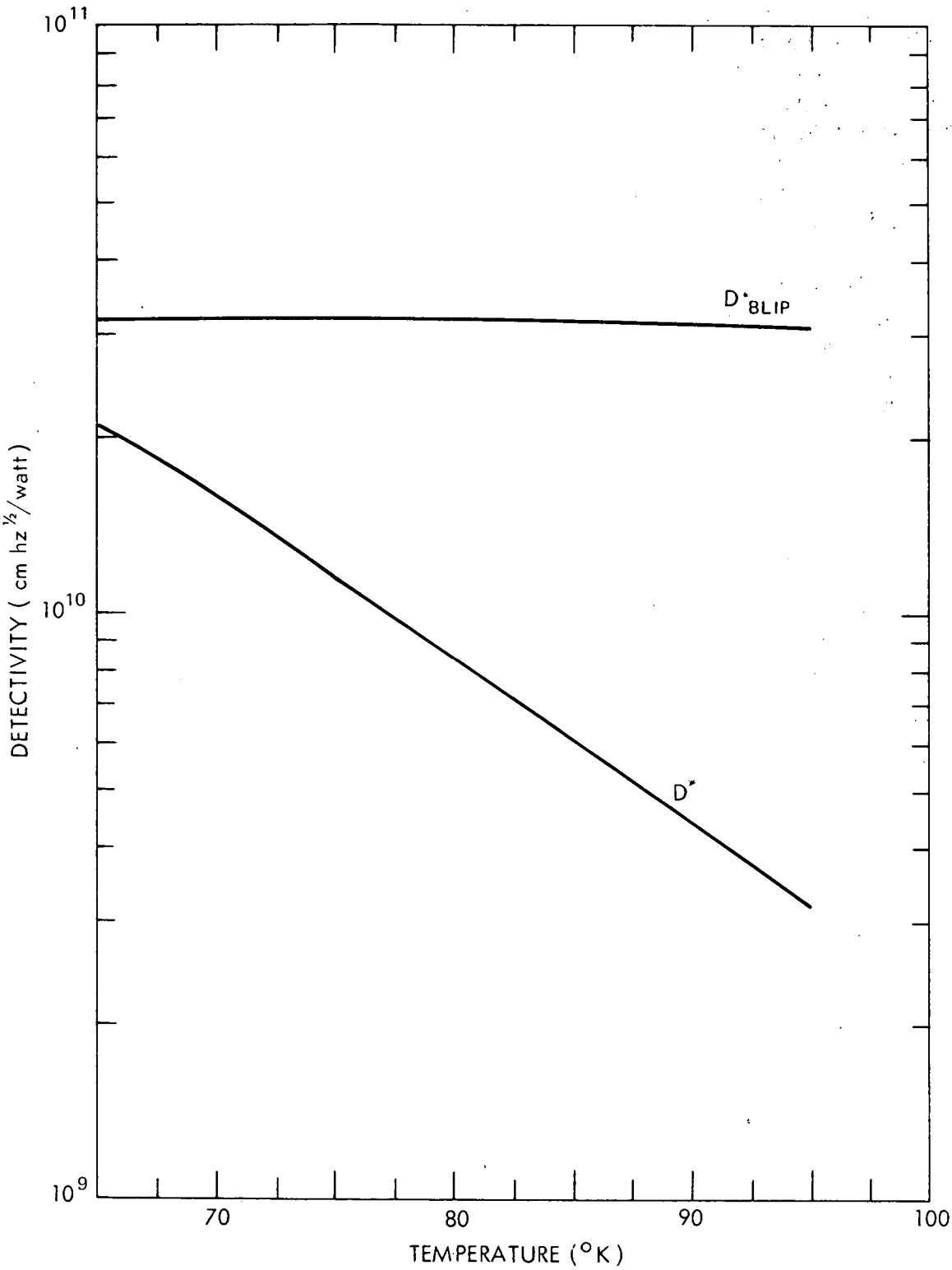

Figure 14. Detectivity vs. Temperature

efficiency (no reflection) of the devices is as high at 45% for HgCdTe and 32% for PbSnTe. Large bandwidth HgCdTe photodiodes must be fabricated in a p on n configuration while those of PbSnTe may be either p on n or n on p. PbSnTe is a more stable material and is less sensitive to variations in crystal composition.

B. Photodiodes for Operation Above 150°K

Diodes fabricated for operating temperatures in excess of 150°K require higher doping concentrations than those designed for operation at low temperature. Dark currents of 10 to 100 milliwatts may be anticipated. This poses a potential heating problem and requires that more than 10 milliwatts local oscillator power be used to achieve quantum noise limited operation. This high local oscillator power will also cause detector heating. The $R_s C$ bandwidth is degraded by about a factor of 3 over that for lower temperature devices by the increase capacitance which is concomitant with increased doping levels. Because electron mobility of PbSnTe decreases more rapidly with temperature than that of HgCdTe transit time limitations on the frequency response in this material become severe for $T > 150°K$. For the same reason the dark currents in PbSnTe as compared to HgCdTe will be somewhat smaller. At temperatures above 150°K thermal noise becomes comparable to dark shot noise and degrades the signal to noise ratio.

VI. REFERENCES

1. Peyton, B.: Phase One Design Report for High Sensitivity Infrared 10.6 Micron Heterodyne Receiver Development, AIL Report 8783-1, Sept. 1969

2. Schmit, J. L. and Stelzer, E. L.: J. Appl. Phys. 40, 4865 (1969)

3. Lennard, J.: private communication

4. Schmit, J. L.: J. Appl. Phys. 41, 2876 (1970)

5. Moss, T. S.: Optical Properties of Semiconductors, Cambridge University Press, Cambridge (1959)

6. Joseph, A.: private communication

7. Soderman, D. A. and Timberlake, A. B.: Mercury Cadmium Telluride Photodiode. Interim Report NASA Contract No. NAS 5-21197 (1971)

8. Melngailis, I. and Harman, T. C.: Single Crystal Lead Tin Chalcogenides, Semiconductors and Semi Metals, Vol. VII, Willardson, R. K. and Beer, A.C., editors

9. Musicant, B. L., Second Quarterly Report, NASA Contract NAS 5-11554 (1969)

10. Peterson, P. E.: J. App. Phys., 41, 3465 (1970)

11. Soderman, D. A., private communication

12. Soderman, D. A., and Pinkston, W. H.: High Speed, High Performance (Hg,Cd)Te Photodiode Detectors Proceedings 1972 Electro-Optical Systems Design Conference (1972)

APPENDIX

Figures A1 and A2 show the number of photons emitted per unit emitter area per second from an ideal blackbody. To determine number of photons incident on a detector of area Ar when the detector field of view, Ω, is filled by the blackbody, multiply by $Ar/\pi\Omega$.

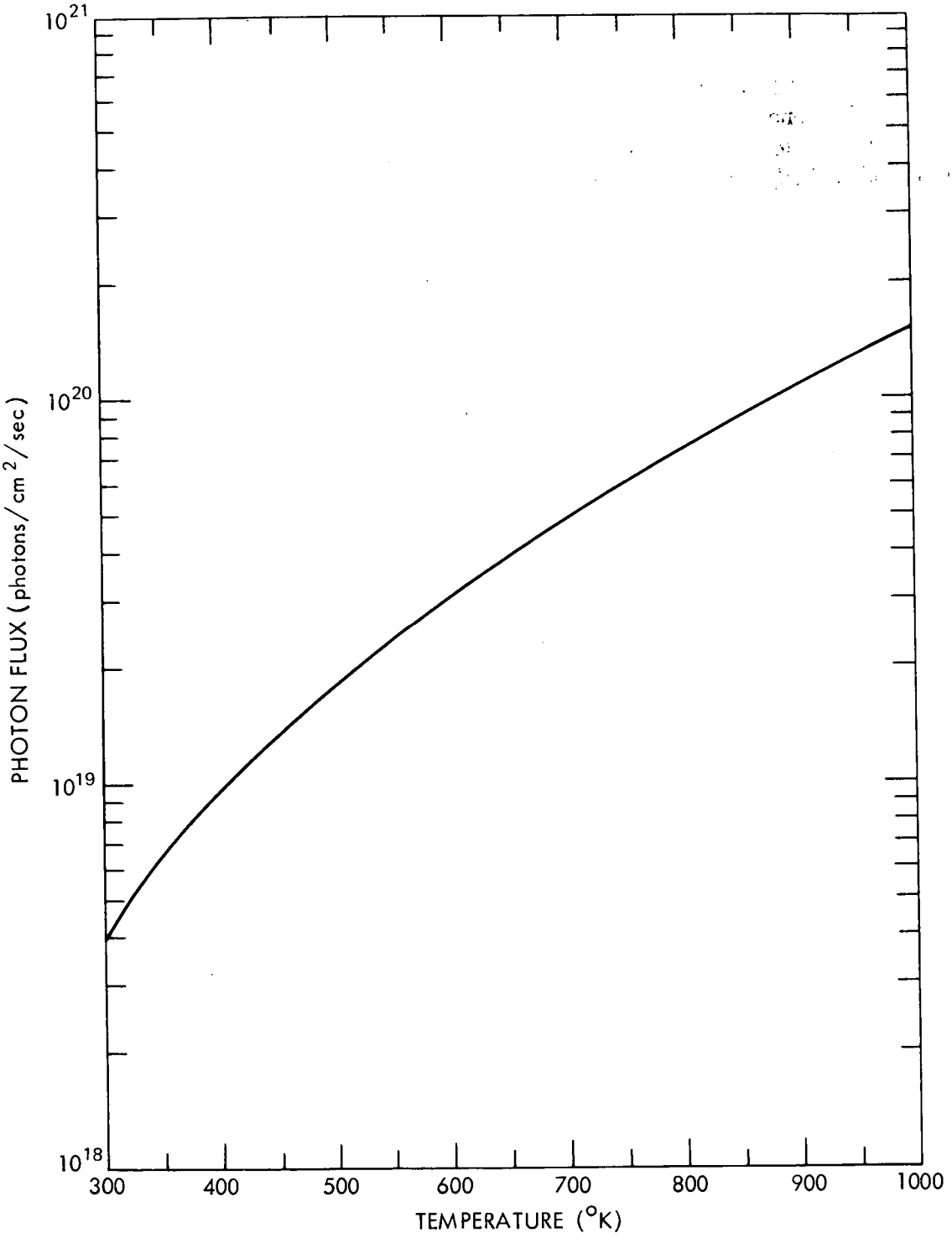

Figure A1. Density of Photons Emitted by Blackbody

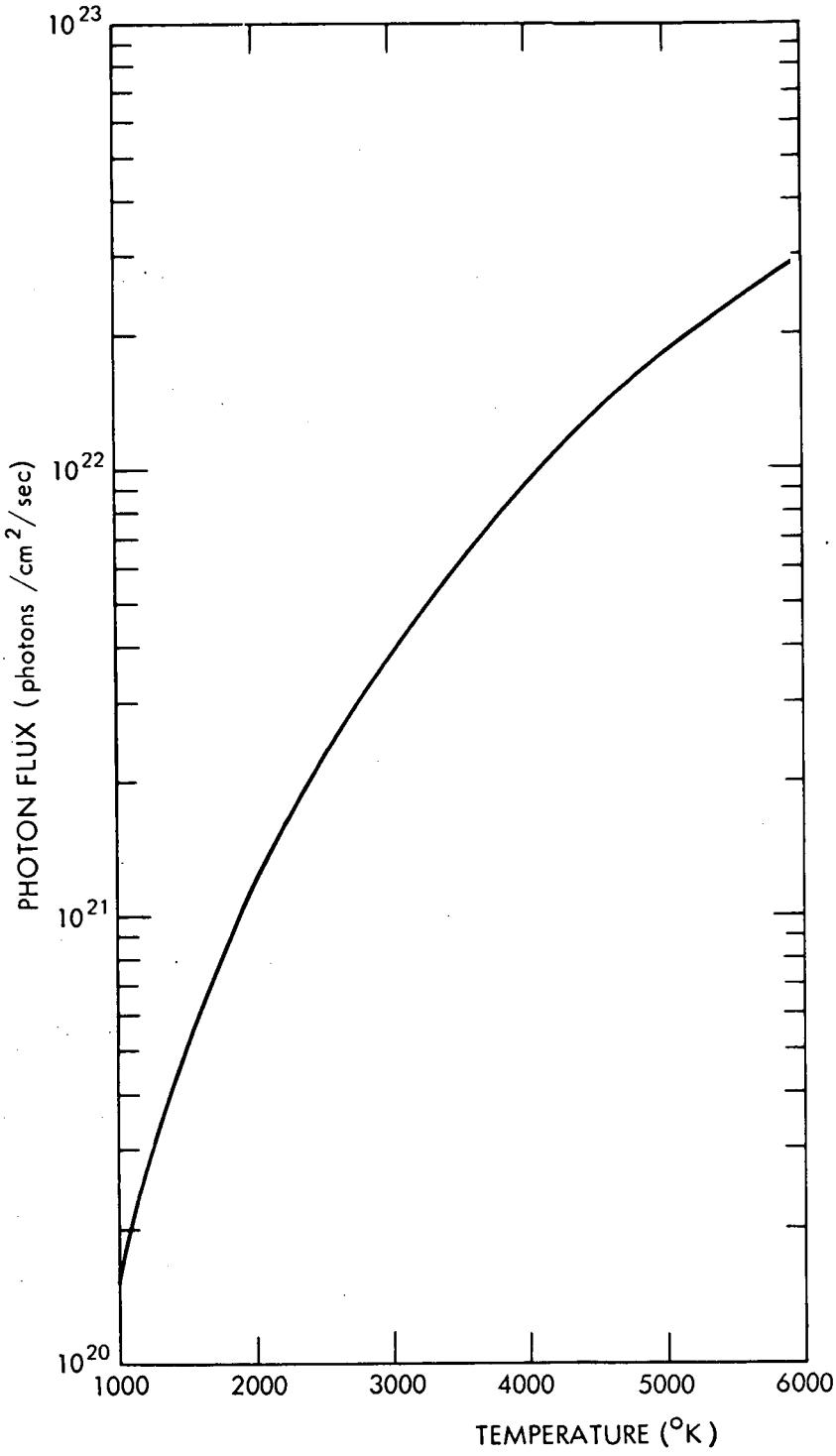

Figure A2. Density of Photons Emitted by Blackbody

NASA–GSFC